This is my blah

A CLAS Proposal for PAC44

Transition Form Factors of the η' and ϕ Mesons with CLAS12

M. C. Kunkel*[†][1], M. J. Amaryan[2], D. Lersch[1], J. Ritman[†][1], S. Schadmand[†][1], X. Song[1]

[1]Forschungszentrum Jülich, Jülich (Germany)
[2]Old Dominion University (U.S.A.)

Abstract

Dalitz decays are radiative decays in which the photon is virtual and subsequently produces an electron positron pair, $P \to l^+ l^- X$. Such decays serve as an important tool used to reveal the internal structure of hadrons and the interaction mechanisms between photons and hadrons. Furthermore, assuming point-like particles, the electromagnetic interaction is calculable within QED by the Kroll-Wada formula. Transition form factors quantify deviations from the QED decay rate. They characterize modifications of the point-like photon-meson vertex due to the structure of the meson. For the η' meson this deviation represents the internal structure of the meson, while for the ϕ meson the deviation represents the transition from $\phi \to \eta$. The transition form factor can be characterized as $\left| F(q^2) \right|$, where q^2 is the square of the invariant mass of the lepton pair, and can be determined by comparing QED predictions to the experimentally measured rate.

Measurements with the highest scientific impact on the determination of the transition form factor have been performed in the space-like region ($q^2 < 0$) in collider experiments. However, due to experimental limitations (e.g. $\pi^{\pm}$ contamination in lepton sample, low branching fractions, external conversion contamination), transition form factors in the time-like region ($q^2 > 0$) have not yet been precisely determined. Recent measurements of the time-like transition form factor for $\eta' \to e^+ e^- \gamma$ have been performed by the BESIII collaboration with insufficient statistical precision, therefore the proper theoretical description cannot be determined.

From previous CLAS analyses using the g12 data set, it was preliminarily shown that measurements of the time-like transition form factor were achievable, but without the statistical precision needed to be competitive. Therefore, we propose to use CLAS12 to focus

---

*Contact person, email: m.kunkel@fz-juelich.de
†Spokesperson

on the dilepton decay channels from the reactions $ep \to e'p\eta'$ and $ep \to e'p\phi$, where $\eta' \to e^+e^-\gamma$ and $\phi \to \eta e^+e^-$. The CLAS12 detector will be used to identify and measure the e^+e^- decay products by means of the High Threshold Cherenkov Counter (HTCC), Pre-Calorimeter (PCAL) and Electromagnetic Calorimeter (EC). The combination of HTCC+PCAL+EC can provide a rejection factor for single $e^\pm/\pi^\pm$ of up to 10^5 for momenta less than 4.9 GeV/c with $\approx 100\%$ efficiency. For dileptons (e^+e^- pairs), this rejection factor will be $\approx 10^{10}$, which enables dilepton studies for branching ratios $\approx 10^{-7}$. Precise determination of momenta and angles of the e^+e^- decay products are the key features available to CLAS12. The momentum and angle of final state photons will be determined in CLAS12 by using the PCAL and EC. Consequently, the photon in the process $\eta' \to e^+e^-\gamma$ and the photons in the process $\phi \to e^+e^-\eta \to e^+e^-\gamma\gamma$ will be detected. Preliminary studies using the CLAS12 simulation suite have shown that a beam time of 100 days, at full luminosity, will accumulate a data sample at least one order of magnitude larger in statistics than the most current $\eta' \to e^+e^-\gamma$ and $\phi \to \eta e^+e^-$ measurement.

Contents

1 Introduction

1.1 Motivation

While very successful in many aspects, the Standard Model of particle physics (SM) leaves a few important questions unanswered. On the one hand, it predicts an amount of matter that survived annihilation after the Big Bang that is many orders of magnitude less compared to what is observed. In addition, since masses of matter particles appear as parameters in the SM, it does not provide any understanding why the values of these masses span so many orders of magnitude. In addition, within the SM phenomena like Dark Matter and Dark Energy can not be explained. These and some more issues suggest that there must be physics beyond the SM, and many experiments world-wide hunt for signals of it.

One of the currently most promising candidates to provide a signal for physics beyond the SM is the muon anomaly $a_\mu = (g-2)/2$. It is a low-energy observable, which can be both measured and computed to high precision [?, ?]. The present experimental value $a_\mu^{\mathrm{EXP}} = 1\,165\,920\,89(63) \times 10^{-11}$ comes from the BNL E821 experiment [?]. This value deviates from the SM prediction by about 3 standard deviations $\Delta a_\mu^{(\mathrm{EXP-SM})} = (287 \pm 80) \times 10^{-11}$ [?] or $= (261 \pm 78) \times 10^{-11}$ [?], depending on how the leading-order hadronic contributions are evaluated. While this discrepancy is not large enough to claim a failure of the SM, it is currently the largest deviation of a SM prediction from an experimental observable. This alone justifies all efforts currently taken to improve both the theoretical as well as the experimental value. New measurements are planned within the next four years at Fermilab/USA [?] and also at JPARC/Japan [?]. The goal of the measurements is to reduce the uncertainty by a factor of four. In parallel the SM prediction needs to be improved in accuracy by at least a factor of two to establish a deviation from the SM for the first time.

The largest uncertainty of the SM prediction comes from the hadronic quantum corrections [?]. At the level of accuracy that is relevant at the moment the hadronic contributions can be split up into the hadronic vacuum polarization (HVP), displayed on the left-hand side of figure 1, and the hadronic light-by-light scattering (HLbL), displayed in the middle of Fig. 1. The most important contribution to the latter comes from the pseudoscalar pole contributions, displayed explicitly on the right-hand side of Fig. 1. For those one expects that the contribution should be largely saturated by the

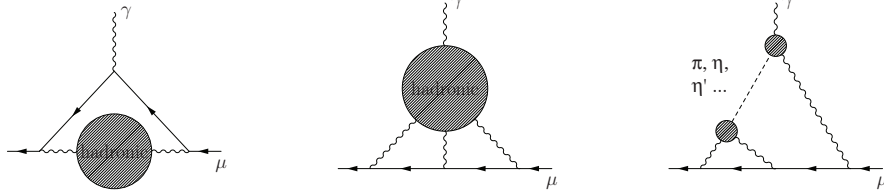lightest exchange particles, namely the π^0, the η and the η'.

Figure 1: Hadronic contributions to a_μ: hadronic vacuum polarization (left diagram), hadronic light-by-light scattering (middle), pion-pole contribution to hadronic light-by-light scattering (right). Full lines with an arrow denote muons, wiggly lines photons, the dashed line a pseudo-scalar meson and shaded blobs a non-pointlike hadronic substructure.

Concerning the SM prediction for a_μ HLbL is suppressed relative to HVP by one power of the electromagnetic fine structure constant [?, ?]. Unfortunately at present it is not possible to straightforwardly calculate the contributions shown in Fig. 1 from first principles analogously to, e.g., the QED corrections, since both processes concern low-energy corrections, i.e. non-perturbative physics. Thus the prime candidate for a SM calculation of hadronic corrections seems to be lattice QCD [?]. However, it is not expected that lattice QCD results for HPV will reach the required accuracy in the foreseeable future. For the HLbL only preliminary lattice-QCD calculations have been reported [?]. In view of the challenges to determine a four-point function that includes in addition disconnected diagrams it is not clear yet when a profound lattice calculation with controlled uncertainties and a reliable error estimate will be available.

Fortunately there is an alternative way to quantify hadronic corrections. It requires both theoretical as well as experimental efforts: Dispersion theory provides a link between particular hadronic cross sections and a_μ—for a discussion of the HVP in this context see Ref. [?], while for HLbL we refer to Refs. [?, ?, ?, ?]. In particular for the latter contribution it allows one to calculate from the transition form factors of the kind π^0, η, $\eta' \to \gamma^*\gamma^*$ the corresponding piece for the meson pole contribution as displayed in the right most diagram of Fig. 1. The measurements proposed here provide important information towards the necessary input needed for the evaluation of the HLbL contribution, since $\eta' \to \gamma^*\gamma$ gives the single off-shell form factor of the η' and $\phi \to \eta\gamma$ additionally provides information on the isoscalar piece of $\eta \to \gamma^*\gamma$ in a different kinematic regime. Additional information on the η and η' form factors can be found from the dispersive methods outlined in Refs. [?, ?, ?, ?, ?]. It appears to be realistic that this joined effort of theory and experiment will provide the improvements necessary to push the SM calculation towards the required accuracy.

1.2 History

In the year 1951, Richard Dalitz published a letter [**?**] in which he calculated the rate for the π^0 decaying into an electron-positron pair (dilepton) and a photon, $\pi^0 \rightarrow e^+ e^- \gamma$. The calculation assumed that the decay proceeded through a two–photon decay in which one of the photons was virtual and converted into an electron-positron pair. This kind of reaction is now known as Dalitz decay. The experimental evidence of this decay process was first observed in emulsion plates exposed to the Chicago cyclotron in 1952 [**?**] and a number of experiments performed over the next ten years verified Dalitz's hypothesis that the $\pi^0 \rightarrow e^+ e^- \gamma$ decay resulted from emission of a virtual photon [**?**, **?**, **?**]. A few years later N. Kroll and W. Wada calculated the framework for Dalitz decays within the QED framework [**?**], and extended the framework to double Dalitz Decays, in which the π^0 decays into two electron-positron pairs via emission of two virtual photons.

Throughout the following years, much work was done to extend the framework of Dalitz decays to heavier mesons, such as η, ω, η', and ϕ. With numerous experimental data taken, it was shown that the shape of the dilepton mass spectrum deviated from the QED predictions. Such deviations are attributed to the meson not being point-like, as calculated in QED, but instead to the internal structure of the meson. The virtual photon, that decayed into a dilepton pair, has the ability to probe the structure of meson because, like its on-shell counterpart, emission of a virtual photon is radiation, which decouples from any strong interaction within the meson when the meson transitions into its decay. Therefore, the information of the transition is encoded into the virtual photon, known as the Transition Form Factor (TFF), and can be characterized as $\left| F(q^2) \right|$, where q^2 is the square of the invariant mass of the lepton pair. The transition form factor can be determined by comparing QED predictions to the experimentally measured rate.

1.3 Proposal

In this proposal we present an experiment to study the η' meson of which decays via Dalitz decay, $\eta \rightarrow e^+ e^- \gamma$. The η is produced via electro-production, $ep \rightarrow ep\eta'$ in Hall B, using the CLAS12 detector. The superior $e^+ e^- / \pi^+ \pi^-$ discrimination of the CLAS12 detector will give access to measurements for which $e^+ e^- / \pi^+ \pi^-$ branching ratios of 10^{12} is achievable. This proposal is organized as follows. In Section 2, an explanation of the kinematics of the decay processes will be given as well as kinematics of main competing backgrounds. In Section **??**, we summarize the current knowledge of Dalitz decays and transition form factors, challenges in dilepton signal quality. Also a brief discussion on past CLAS analysis will be given, along with and how the CLAS12 detector can surpass the current challenges in measuring a TFF,

for η', of low statistical error. In Section 3 a description of the analysis techniques that have been used and will be used in a CLAS12 measurement. Also in Section 3, an explanation of the Monte-Carlo simulations that were performed to extract the acceptances will be given as well as a calculation of expected yield and a validity check on the expected yield from previous CLAS analyses. In Section 5 we present the beam time request.

2 Kinematics

The channel proposed to be studied is

$$e(k) + p(p) \rightarrow e'(k') + p'(p') + \eta'(\nu) \tag{1}$$

where k, k', p, p' are the four–momenta of the incident lepton, outgoing lepton, target proton and scattered proton respectively. The virtual photon in the production is defined as $q = k - k'$ with energy $v = \frac{pq}{m_p} = E - E'$. The quantity $\eta'(\nu)$ is the electro-produced meson. Production mechanisms of similar mesons have been already proposed in previous proposals [?, ?] and are scheduled to run in conjunction with RunGroupA, the same run group requested for in this proposal. The main decays studied for this proposal are:

$$\eta' \rightarrow \gamma\gamma \rightarrow e^+e^-\gamma \tag{2}$$
$$\eta' \rightarrow \gamma\gamma^\star \rightarrow \gamma e^+e^- \tag{3}$$

i.e. when a pseudoscalar meson, $P_p(\eta')$, decays via two photons (Eq. 2) and one photon converts into an e^+e^- pair due to E.M. processes through matter, this is conventionally known as external conversions. This decay channel will be the main background contribution and is further discussed in Sec 2.3. The Dalitz decay(Eq. 3), or internal conversion, is when the $P_p(\eta')$ decays via a real photon and a virtual photon, which decays into an e^+e^- pair. Figure 2 illustrates the Feynman diagrams for the pseudoscalar "two photon decay" and "Dalitz decay". A full derivation of the external conversion and Dalitz decay are given in the Appendix A.
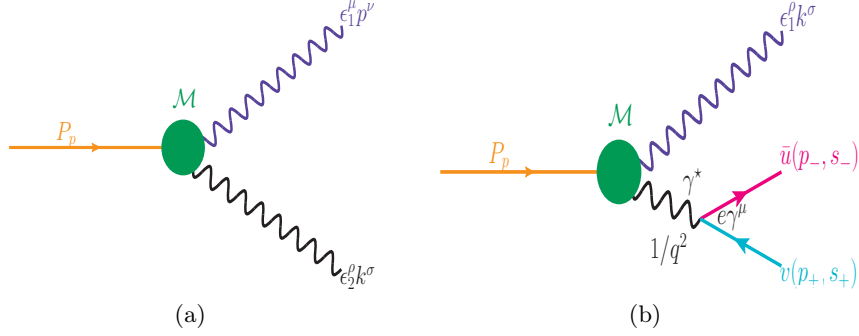
Figure 2: Feynman diagram of $P_p(\eta')$ two photon decay (a), ϵ_1 and ϵ_2 are the polarizations, p and k are 4-momenta of the photons. Feynman diagram of $P_p(\eta')$ Dalitz decay (b), the variable $s_\pm$ are the spin helicities of the outgoing leptons $l^\pm$ with 4-momenta $p_\pm$ and ϵ is the polarization of the outgoing photon with 4-momenta k. In both diagrams $\mathcal{M}$ is the form factor.

2.1 The Dalitz Decay

The Dalitz decay of mesons is dependent on the spin of the meson. For pseudoscalar meson the decay rate is derived in A.3 and is expressed as:

$$\frac{d\Gamma_{e^+e^-\gamma}}{\Gamma_{\gamma\gamma}dq^2} = \frac{2\alpha}{3\pi}\frac{1}{q^2}\left(1 - \frac{q^2}{m_p^2}\right)^3\left(1 + \frac{2m_l^2}{q^2}\right)\left(1 - \frac{4m_l^2}{q^2}\right)^{\frac{1}{2}} \qquad (4)$$

which is the Kroll-Wada equation founded in [?, ?]. An example of QED expectation for η' is shown in Fig. 3.

2.2 Form Factor

It has been experimentally observed that the shape of the dilepton mass spectrum deviates significantly from the QED predictions, displaying a rise at larger dilepton mass. Therefore, the form factor $M_P(p^2, k^2 = 0)$ or $M_P(p_1^2, p_2^2)$ can be written as follows:

$$M_P \to M_P' \times \left|F(q^2)\right| \ , \qquad (5)$$

where M_P' is the decay constant of two photons or η photon (as mentioned in Sec. A.1), while $\left|F(q^2)\right|$ is called the transition form factor, which defines the electromagnetic space structure of the meson. According to that, the $\eta' \to e^+e^-\gamma$ the decay rate modifies as;

$$\frac{d\Gamma_{e^+e^-\gamma}}{\Gamma_{\gamma\gamma}dq^2} = \frac{2\alpha}{3\pi}\frac{1}{q^2}\left(1 - \frac{q^2}{m_p^2}\right)^3\left(1 + \frac{2m_l^2}{q^2}\right)\left(1 - \frac{4m_l^2}{q^2}\right)^{\frac{1}{2}}\left|F(q^2)\right|^2 \ , \qquad (6)$$

7

First observations were described with standard vector meson dominance (VMD) where the virtual photon can stem from a intermediate vector mesons. The value of $\left|F(q^2)\right|$ can be directly measured by comparing QED predictions to the measured rate [?].

$$\frac{d\Gamma(A \to B + l^+l^-)}{dq^2\Gamma(A \to B\gamma)} = \left[\frac{d\Gamma}{dq^2}\right]_{\text{QED}} \cdot \left|F(q^2)\right|^2 \qquad (7)$$

or by performing a line shape analysis on the l^+l^- invariant mass using assumptions on the structure of $\left|F(q^2)\right|$. One such assumption for $\left|F(q^2)\right|$ is the dipole approximation from the VMD model, which can be parametrized as:

$$F(q^2) = \frac{1}{1 - q^2/\Lambda^2} \qquad (8)$$

where the parameter Λ corresponds to the mass for the effective contributing vector meson.

The slope of the transition form factor, b, is defined as:

$$b \equiv \frac{dF}{dq^2}|_{q^2=0}. \qquad (9)$$

and characterizes the intrinsic spatial charge radius for the η' meson, and the $\phi \to \eta$ transition for the ϕ meson. Several theoretical approaches have been developed to describe the transition form factor and are listed in Tab. 1.

Approach	slope parameter ($b_{\eta'}$)
Dispersion	$1.53^{+0.15}_{-0.08}\text{GeV}^{-2}$
Chiral Perturbation	1.6GeV^{-2}
VMD	1.45GeV^{-2}

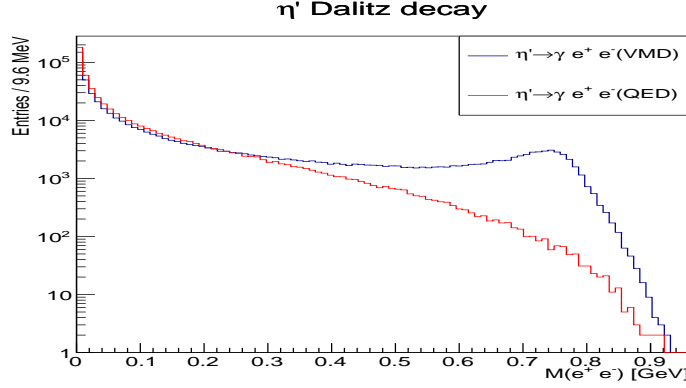Table 1: Theoretical approaches to describe the transition form factor

Figure 3: Example of Dalitz spectra for η' using only QED(red) and the deviation from QED using the VMD parameterization(blue) with 500K Dalitz events generated **??**.

2.3 Photon Conversion to e^+e^- Pairs

When a photon travels through matter at energies greater than 100 MeV, it can convert into an electron-positron pair. The process of pair production, $\gamma Z \rightarrow Z e^+ e^-$, occurs when a photon with $E_0 > 2 m_e c^2$ converts into an electron and a positron. The cross section for this process can be written as;

$$\sigma_{\gamma \rightarrow e^+ e^-} = \frac{A}{N_A \rho \lambda_\gamma} \ , \ \lambda_\gamma = \frac{9}{7} X_0 \tag{10}$$

where λ is the interaction length, or mean free path, ρ is the density of the material, N_A is Avogadro's number and A is the atomic mass of the material. The probability of pair production to occur is solely based on X_0, the radiation length of the medium and this probability can be expressed as;

$$\frac{dP}{dx} = \frac{1}{\lambda_\gamma} \exp(\frac{-x}{\lambda_\gamma}) \ . \tag{11}$$

Using the ratio, $\frac{\Gamma_{\eta' \rightarrow e^+ e^- \gamma}}{\Gamma_{\eta' \rightarrow \gamma \gamma}} = 2.13 \cdot 10^{-2}$, that has been preliminary measured by CLAS, which is consistent with [**?**], the probability of pair production when a photon, from the $\eta' \rightarrow \gamma \gamma$ decay, traveling though 5 cm of liquid hydrogen, ℓH_2, is shown in Fig. 4 as well as the number of $\eta' \rightarrow \gamma \gamma \rightarrow e^+ e^- \gamma$ / $100 \eta' \rightarrow e^+ e^- \gamma$. Since CLAS12 has a vertex resolution of $\approx$1 mm the probability of pair production traveling through 10 mm is shown in Fig. 5. Therefore, a 1 mm cut on the primary vertex will yield a contamination of $\approx$ one externally converted $e^+ e^-$ from $\eta' \rightarrow \gamma \gamma \rightarrow e^+ e^- \gamma$ per Dalitz decays $100 \eta' \rightarrow e^+ e^- \gamma$ This type of subprocess mimics the Dalitz decay $\eta' \rightarrow e^+ e^- \gamma$, described in Sec. A.3. Since there are two photons with equal probability
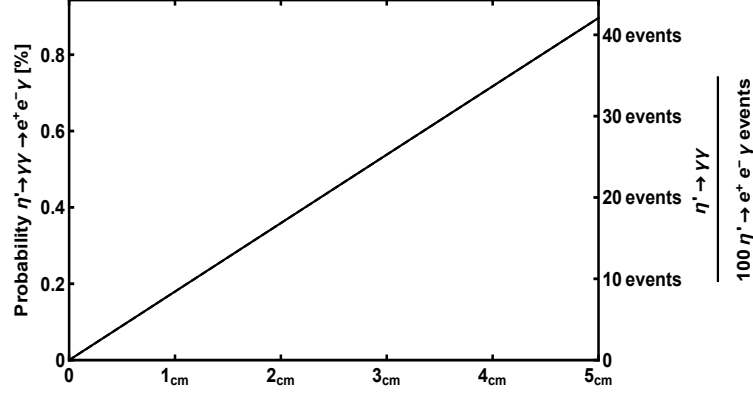
9

Figure 4: (Left axis)Probability of pair production, $\gamma \to e^+ e^-$; (Right axis) number of $\eta' \to \gamma\gamma \to e^+ e^- \gamma$ / $100\eta' \to e^+ e^- \gamma$ as a function of distance in liquid hydrogen.
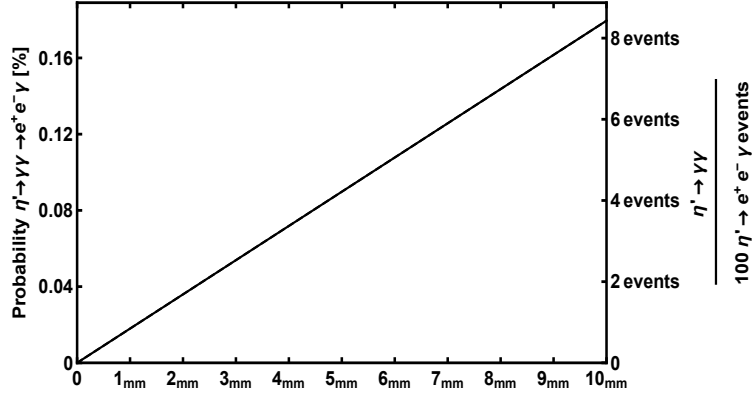

Figure 5: (Left axis)Probability of pair production, $\gamma \to e^+ e^-$; (Right axis) number of $\eta' \to \gamma\gamma \to e^+ e^- \gamma$ / $100\eta' \to e^+ e^- \gamma$ as a function of distance in liquid hydrogen.

of conversion for $\eta' \to \gamma\gamma$, the total probabilities shown is for when either photon externally converts. From multiple scattering effects the $e^+ e^-$ from a converted photon will obtain a mass distribution. Simulations of photons from η' and ϕ radiative decays traversing through 1 mm of ℓH_2 show that the $e^+ e^-$ can obtain a maximum mass of ~ 0.14 GeV.

2.4   Summary

The $\gamma\gamma$ decay and the $\gamma^\star\gamma$ decay have different branching ratios. This difference is attributed to the factor of α along with a q^2 dependence calculated
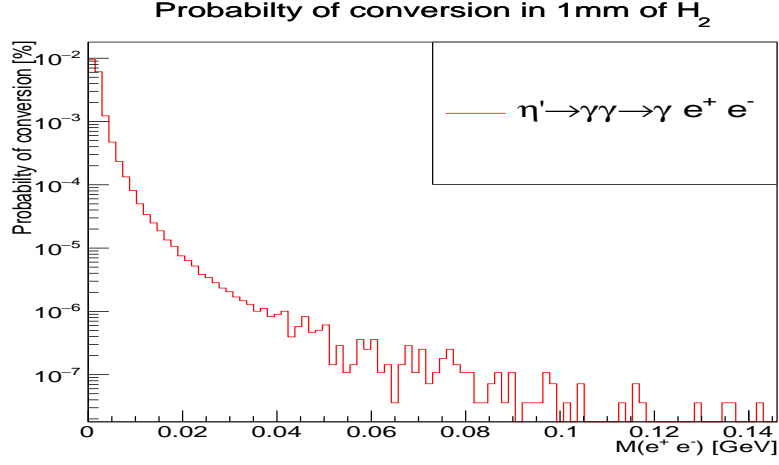
Probabilty of conversion in 1mm of H$_2$

Figure 6: Probability of pair production in 1 mm of ℓH_2 for $\eta' \to \gamma\gamma$ vs. $M(e^+e^-)$.

in the Dalitz decay. However, due to the probability of a photon converting into an electron-positron pair in ℓH_2, the total amount of e^+e^- pairs produced via photon conversion can contaminate the measurement of the form factor. The CLAS detector will have vertex resolution of ~1 mm, therefore the amount of contamination of externally converted pairs will be minimized by the vertex position of the e^+e^- pair. An example of the total contamination, in the Dalitz spectrum, from external conversion within 1 mm of the primary vertex can be seen in Fig. 7.
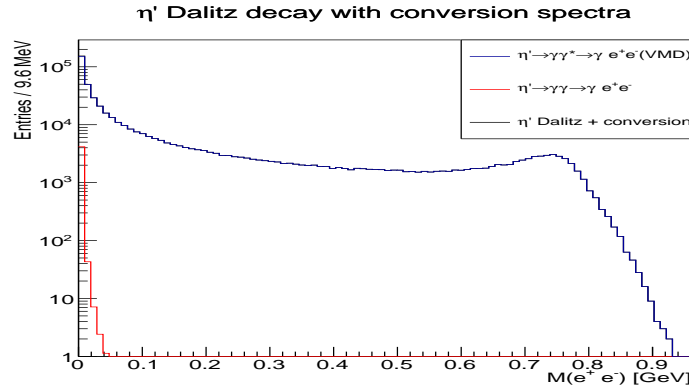

η' Dalitz decay with conversion spectra

Figure 7: Example of Dalitz and conversion spectra for η' with 500K Dalitz events generated and $\sim 2.35 \cdot 10^7$ $\eta' \to \gamma\gamma$ generated.

11

3 Measurement

This section is a description on how the $\eta \to e^+e^-\gamma$ was simulated and reconstructed for this CLAS12 proposal.

3.1 Simulation and Reconstruction

To simulate the reaction in Eq. 1, the program PLUTO++ [?] was utilize for its ability to simulate the decays of those according to QED, Vector Meson Dominance or a user inputted TFF. For reconstruction of the desired topologies, the CLAS12 FASTMC [?] and GEMC were used, in which $\sim 9 \cdot 10^6$ events were generated for $\eta' \to e^+e^-\gamma$ and then simulated with FASTMC/GEMC at 75% torus field. The EC efficiency was calculated by comparing GEMC (GEANT4) simulations with FASTMC. This EC efficiency was also calculated with the g12 data set and was identical to the comparison of the two simulation methods. The accpetance for this propose was performed using FASTMC.

An extra FASTMC simulation was performed for the torus field setting of 100% to show the effects of the magnetic field on the lepton acceptance. All detector efficiencies are assumed to be 100% except the EC efficiency, in which an efficiency of 10% was factored for each detected lepton and photon.

The production of each particle was weighted by photo-production differential cross-sections, $\frac{d\sigma}{d\Omega}(v, \cos\theta_{cm})$, published in [?], where v is the virtual photon energy. This was done to achieve a quasi realistic model of the production. The e^+e^- decay spectrum, of each meson, was weighted via the VMD model (including QED predictions). Another simulation was performed using a flat $M(e^+e^-)$ distribution (No QED, No VMD) to analyze any effects of the model on the e^+e^- acceptance. The analysis showed that this acceptance was independent of the decay model, see Fig.10 and Fig.11.

3.1.1 Trigger Requirements

The standard CLAS12 electron trigger (HTCC(Nphe>2) * [(PCAL+EC)>1.0 GeV] is sufficient for this types of analysis. It has been shown in previous proposals [?, ?] that the rate of the standard electron trigger will be 6 kHz, which the expected data acquisition (DAQ) readout rate is 10 kHz.

3.1.2 Detection of e^+e^- Events

Electron/positron ID will include responses from the HTCC, PCAL and EC calorimeters. The energy information of the PCAL and the inner and outer parts of EC will be used to compare the total energy deposition with the momentum measured in the DC ($\alpha * (E_{Pcal} + E_{ECin} + E_{ECout}) \sim P_{DC}$), where α is a scaling factor.

3.1.3 Particle Identification

The η' meson have pion decay modes, which are orders of magnitude greater than the Dalitz decay. For example, the ratio $\Gamma\pi^+\pi^-\gamma/\Gamma e^+e^-\gamma$ is $6.2 \cdot 10^2$. Electrons/positrons will be identified by using the information from the detectors described above. The expected $e^\pm/\pi^\pm$ rejection factor for single particles (p<4.9 GeV) is 10^3 for the HTCC, while the PCAL+EC can provide an additional factor of 10^2. Combining both methods yields a $e^\pm/\pi^\pm$ rejection factor of 10^5 which results in a $e^+e^-/\pi^+\pi^-$ rejection factor of 10^{10}. Therefore, the amount of $\pi^+\pi^-$ background in the $M(e^+e^-)$ spectrum will be $\approx 6.2\cdot 10^2/10^{10} = 6.2\cdot 10^{-8}$. A detailed explanation of particle identification for e^+e^- pairs can be found in [**?**].

3.1.4 Acceptance

An exclusive reconstruction scheme

$$ep \rightarrow e'p\eta' \rightarrow pe^+e^-\gamma \tag{12}$$

where all final state particle are detected, as well as an inclusive reconstruction scheme

$$ep \rightarrow e'p\eta' \rightarrow e^+e^-\gamma(p) \tag{13}$$

where the proton was not detected, was analyzed. Figure 8 and Fig. 9 show the generated e^+e^- spectrum along with the accepted events for both reconstruction schemes for the VMD $M(e^+e^-)$ weighted MC and the flat $M(e^+e^-)$ weight MC. The acceptance was calculated by dividing the accepted events by the generated events, per $M(e^+e^-)$ bin. The η' Dalitz decay acceptance can be seen in Fig.10.

Figure 8: Generated events (Top), accepted events for an exclusive (Middle), inclusive(Bottom) reconstruction schemes as a function of $M(e^+e^-)$. In all panels a VMD decay model was employed
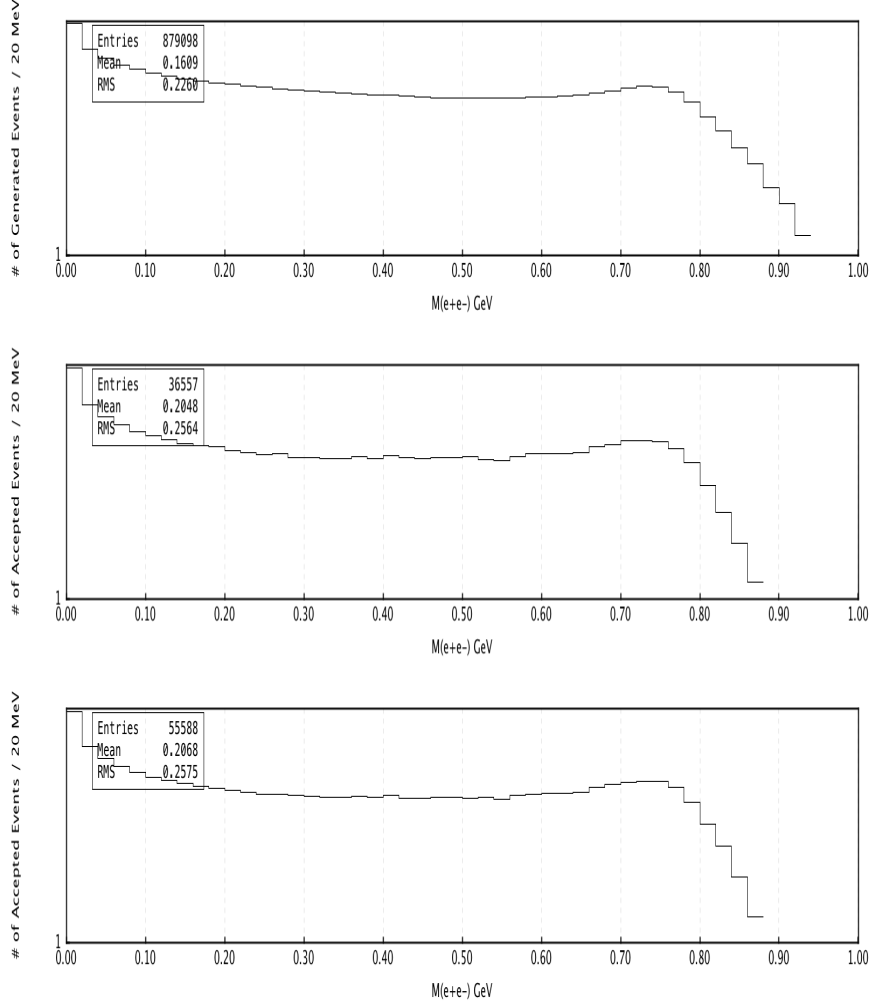
14
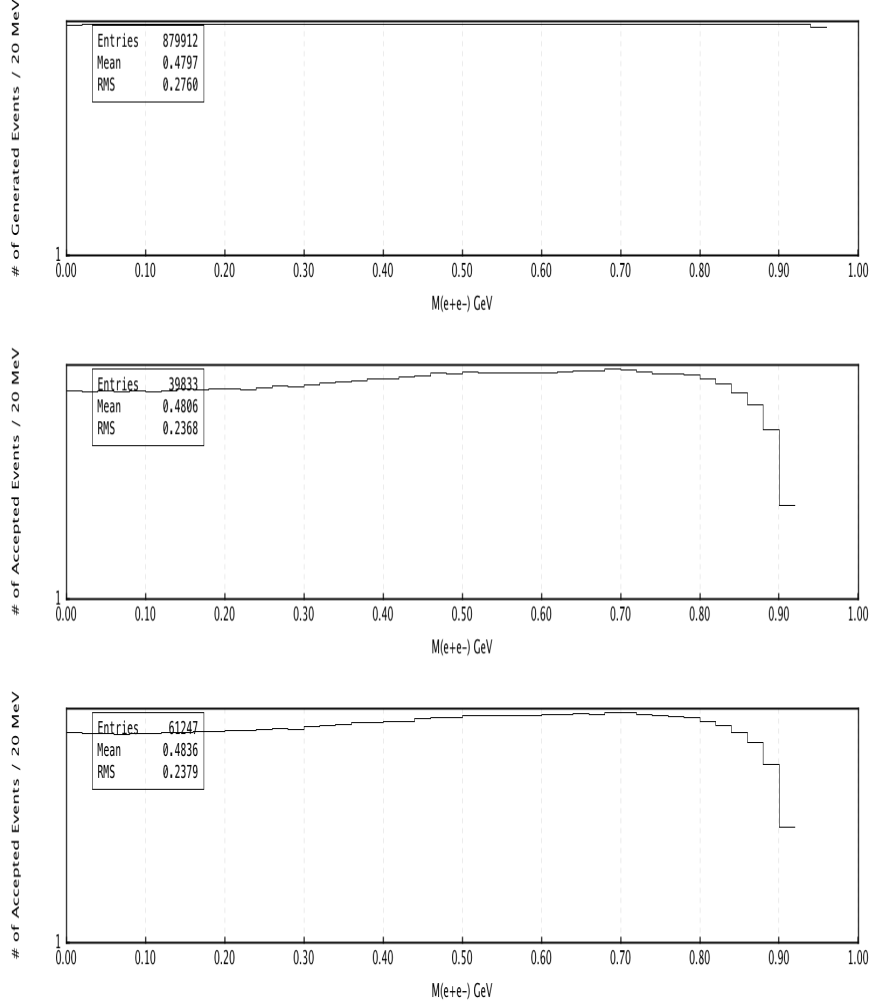
Figure 9: Generated events (Top), accepted events for an exclusive (Middle), inclusive(Bottom) reconstruction schemes as a function of $M(e^+e^-)$. In all panels a Flat e^+e^- decay model was employed

15

Figure 10: Acceptance using a VMD decay model, as a function of $M(e^+e^-)$ for the exclusive (Top) and inclusive reconstruction scheme(Bottom).

Figure 11: Acceptance using a flat e^+e^- decay model, as a function of $M(e^+e^-)$ for the exclusive (Top) and inclusive reconstruction scheme(Bottom).

3.2 Calculating Expected Yield

3.2.1 Calculating Photon Flux

A simple method for calculating the photon flux in CLAS12 is as follows; Using the fact that g12 had a photon flux of $7 \cdot 10^7$ γ/s on a Au radiator of

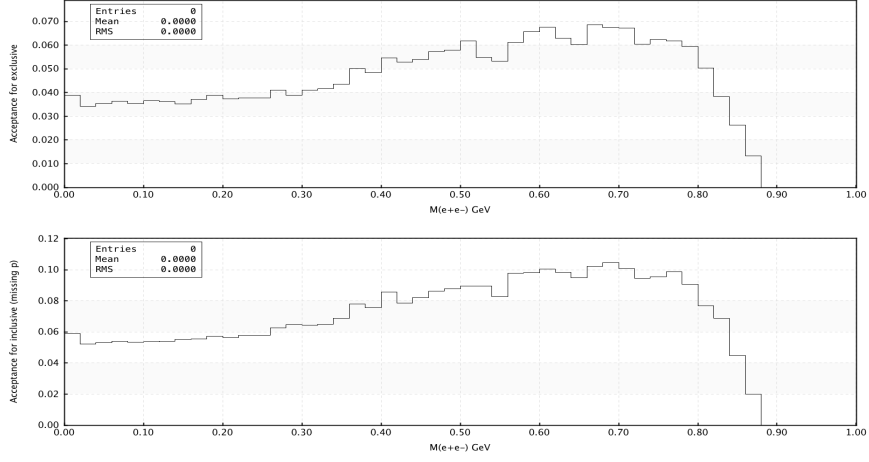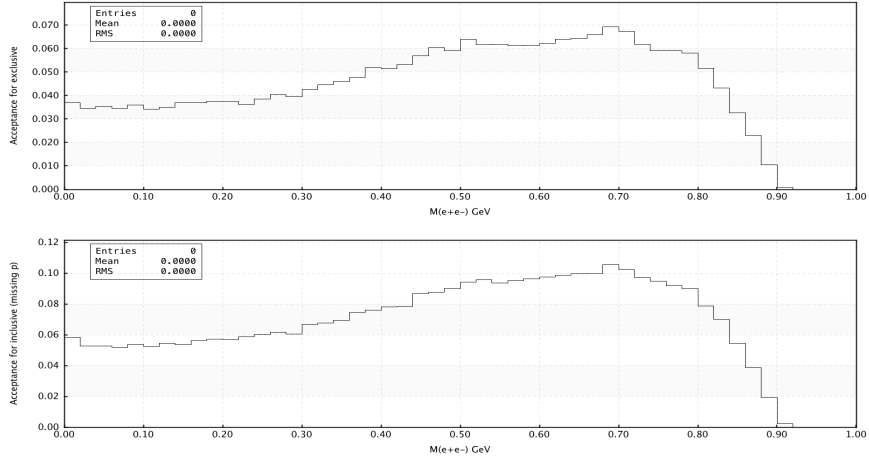$10^{-4}\chi_0$ an expected $\sim 4 \cdot 10^9 \gamma/$s will be seen in CLAS12 at $\mathcal{L} = 10^{35}\mathrm{cm}^{-2}\mathrm{s}^{-1}$ on a 5 cm ℓH_2 target which is $\sim 5.7 \cdot 10^{-3}\chi_0$. This number has been independently confirmed in a previous CLAS proposal [?].

3.2.2 Expected Results

The average number of meson $\rightarrow e^+e^-X$ expected in CLAS12 can be calculated as:

$$\bar{N}(e^+e^-)_{\mathrm{meson}\rightarrow e^+e^-X} = \Phi\epsilon(e^+e^-)\bar{\sigma}\rho_{\ell_{H_2}}\ell_{target}N_A\frac{\Gamma_{\mathrm{tot_{meson}}}}{\Gamma_{\mathrm{meson}\rightarrow e^+e^-X}} \ , \quad (14)$$

where Φ is the photon flux estimated in Sec. 3.2.1, ϵ is the acceptance, $\bar{\sigma}$ is the total cross-section, $\rho_{\ell_{H_2}}$ is the atomic density of ℓ_{H_2}, ℓ_{target} is the target length, N_A is Avogadro's constant, and $\frac{\Gamma_{\mathrm{tot_{meson}}}}{\Gamma_{\mathrm{meson}\rightarrow e^+e^-X}}$ is the total branching fraction of the meson decaying into e^+e^-X. Using the lepton acceptance shown is Sec. 3.1.4 the average number of η' per $M(e^+e^-)$ can be seen in Fig. 12.
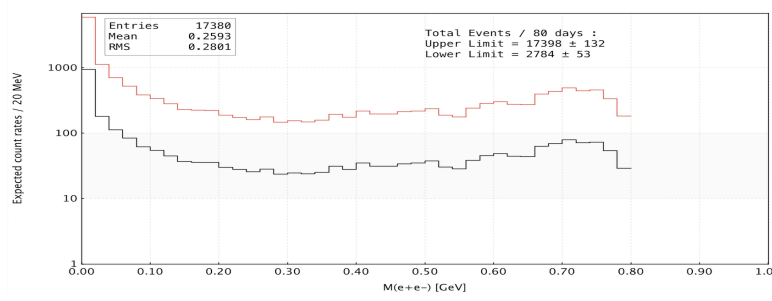
(a)
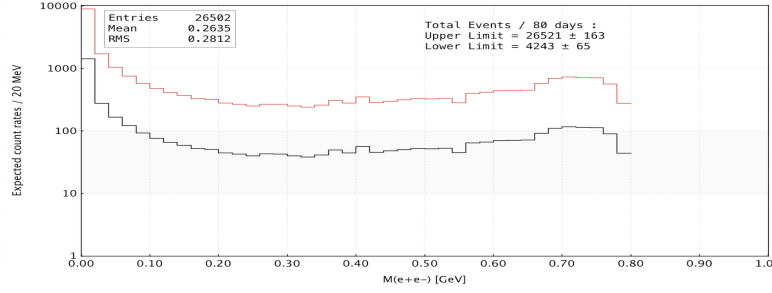
(b)

Figure 12: Count rates for the exclusive (a) and inclusive (b). For both plots the photon detection efficiency was assumed to be between 10%(Red) and 2%(Black).

Integrating over $M(e^+e^-)$, the expected yield calculates to be $17,398$ events for exclusive scheme and $26,521$ events for the inclusive scheme. This would increase the world statistics by a factor of ~ 20 and ~ 30 respectively. Table 2 and Tab. 3 in App. B depicts the upper and lower amount of e^+e^- expected from 80 days of beam time for two torus fields of 75% and 100% respectively.

3.3 Realistic Yield

As a reality check, lets compute the number of $\eta' \to e^+e^-\gamma$ that g12 would have seen, had the experiment ran for 80 days with a real photon flux as calculated for CLAS12 (Sec. 3.2.1). The 89 $\eta' \to e^+e^-\gamma$ events produced in g12 were recorded when the e^+e^- trigger was established. This time was

18

66% of the total 44 days, which is ~ 29 days. The total integrated flux measured during this time was $\sim 8.8 \cdot 10^{13}$ photons. Therefore, in 80 days the total integrated flux would have been $\sim 2.4 \cdot 10^{14}$ and the total number of $\eta' \to e^+ e^- \gamma$ events recorded would have been 242. The ratio of g12 total flux at 80 days per CLAS12 real photon flux is $2.73 \cdot 10^{16}/2.4 \cdot 10^{14} \sim 114$. Therefore g12 would have recorded $114 \cdot 242 = 27590 \ \eta' \to e^+ e^- \gamma$ events, which is consistent with what is proposed to be measured with 80days, in the inclusive reconstruction scheme for either torus field setting. See Sec. B for total count rates.

3.4 Acceptance at 100% Torus field

An addition simulation was performed using the same generated data shown above, the difference being the setting of the torus magnetic field. Below, in Fig. 13, the ratio of the lepton acceptance for the two different torus settings is depicted.

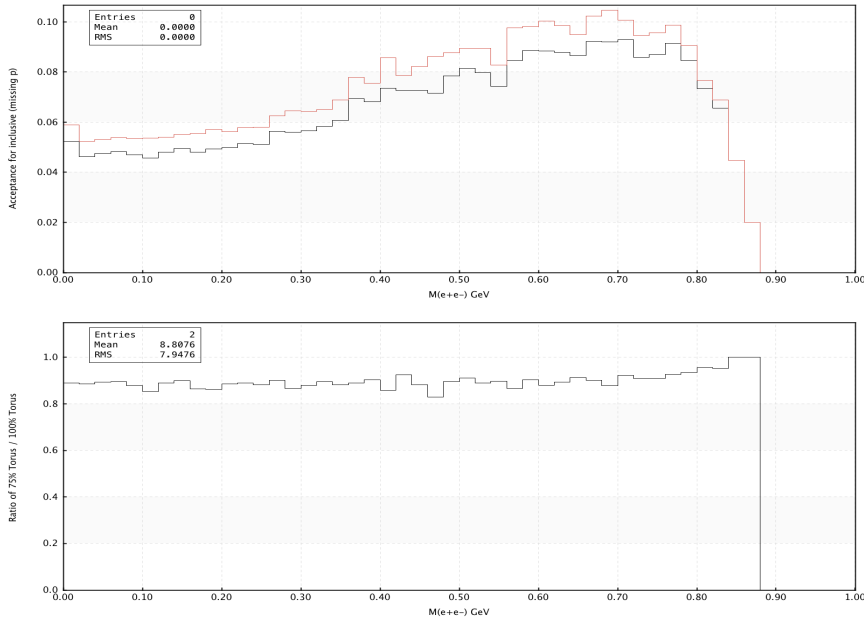Figure 13: Acceptance using a VMD decay model, as a function of $M(e^+ e^-)$ for the inclusive scheme(Top). The torus field was set to 75%(red) as well as 100%(black). Ratio of the acceptances plotted above (75%/100%)(Bottom).

3.5 Expected Systematic Uncertainties

The major sources of systematic uncertainties are the acceptance and particle identification. The lepton acceptance uncertainty is estimated to be $\lesssim$

5% which was observed in former CLAS experiments. The lepton identification uncertainty will arise from the performance of the HTCC, PCAL and EC. From simulation studies performed for this proposal, all leptons and final state photons are detected within the geometric space of the PCAL+EC with hit coincidences in both. Furthermore, all leptons, within a few percent, that were detected in the PCAL+EC were also detected in the HTCC. Further systematics from pion contamination are mitigated by the pion rejection factor described above. Systematics related to external photon conversion are minimal due to the 1 mm resolution of the primary vertex given by the Silicon Vertex Tracker (SVT) as shown in Sec 2.3. Any Bethe-Heitler contributions are negligible when utilizing and exclusive meson reconstruction scheme.

4 Manpower

To analyze the $\eta' \rightarrow e^+ e^- \gamma$ and $\phi \rightarrow e^+ e^- \eta$ decays, a minimum of one postdoctoral associate and one graduate student will be needed to perform the following tasks:

or allotted?

- Aide in the calibration of RunGroupA

- Skim and analyze the $e^+ e^-$ data

- Simulate and correct the data

- Write publications of the results

5 Beam Time Request

With this proposal and beam time request, we ask for 100 days of beam time. Of the 100 days, 80 days will be dedicated to the production beam time with the standard CLAS setup, at full luminosity ($\sim 10^{35} \text{cm}^{-2} \text{s}^{-1}$) with 75% torus field. The remaining 20 days will be dedicated to optimizing and testing the trigger set-up (HTCC +PCAL + EC). This request should provide a competitive data sample of $\eta' \rightarrow e^+ e^- \gamma$ and $\phi \rightarrow e^+ e^- \eta$. The CLAS12 configuration we propose for the measurement of the transition form factors is compatible with the experimental setup already established by Run Group A.

Appendices

A   Decay Kinematics

A.1 $\eta' \to \gamma\gamma$ Decay

As shown in Fig. 2a, the two photon decay can be expressed in terms of the respective momentum, $P_p(\eta') \to \gamma(\epsilon_1, p)\gamma(\epsilon_2, k)$, where ϵ_1 and ϵ_2 are the polarizations of the photons with 4-momenta p and k. Dropping the nomenclature (η') in $P_p(\eta')$, the four momentum of the decaying meson is $P_p = p+k$. Using the Feynman rules as given in [?]and [?], which are Lorentz and gauge invariant and also parity conserving, the amplitude can be solved to be:

$$\mathcal{M}(P_P \to \gamma(\epsilon_1, p)\gamma(\epsilon_2, k)) = M_P(p^2 = 0, k^2 = 0)\varepsilon_{\mu\nu\rho\sigma}\epsilon_1^\mu p^\nu \epsilon_2^\rho k^\sigma \qquad (15)$$

where $\varepsilon_{\mu\nu\rho\sigma}$ is the antisymmetric metric tensor. The form factor, $M_P(p^2 = 0, k^2 = 0)$, contains information of the decaying meson and since the decay products are on-shell photons, which are massless, M_P is a constant given as;

$$M_P = \begin{cases} \dfrac{\alpha}{\pi f_\pi} & \text{if } P = \eta'; \\ \dfrac{\alpha}{\pi f_\pi}\dfrac{1}{\sqrt{3}}\left(\dfrac{f_\pi}{f_8}\cos\theta_{mix} - 2\sqrt{2}\dfrac{f_\pi}{f_0}\sin\theta_{mix}\right) & \text{if } P = \eta; \\ \dfrac{\alpha}{\pi f_\pi}\dfrac{1}{\sqrt{3}}\left(\dfrac{f_\pi}{f_8}\sin\theta_{mix} + 2\sqrt{2}\dfrac{f_\pi}{f_0}\cos\theta_{mix}\right) & \text{if } P = \eta' \end{cases} \qquad (16)$$

where $\alpha = e^2/4\pi \approx 1/137$ is the fine structure constant, $f_\pi \approx 92.4\,\text{MeV}$ is the physical value of the pion-decay constant and $f_0 \approx 1.04 f_\pi$ and $f_8 \approx 1.3 f_\pi$ are the singlet and octet Pseudo-Goldstone meson decay constants.

A.1.1   *Squared Matrix Element*

The squared matrix element of the decay $P_P \to \gamma(\epsilon_1, p)\gamma(\epsilon_2, k)$ is given by

$$|\mathcal{M}(P_P \to \gamma(\epsilon_1, p)\gamma(\epsilon_2, k))|^2 = |M_P|^2\,\varepsilon_{\mu\nu\rho\sigma}\varepsilon_{\mu'\nu'\rho'\sigma'}\epsilon_1^\mu p^\nu \epsilon_2^\rho k^\sigma \epsilon_1^{\mu'} p^{\nu'} \epsilon_2^{\rho'} k^{\sigma'}$$
$$(17)$$

which can be simplified to;

$$|\mathcal{M}(P_P \to \gamma(p)\gamma(k))|^2 = |M_P|^2\,\varepsilon_{\mu\nu\rho\sigma}\varepsilon^{\mu\nu}{}_{\rho'\sigma'}p^\rho p^{\rho'} k^\sigma k^{\sigma'} \qquad (18)$$

by assuming that the polarizations of the photons remain unobserved, as they are in CLAS. Therefore the photon polarization vectors can be summed using Eq. 5.75 from [?] which reads as;

$$\sum_{polarizations} \epsilon_\mu \epsilon_{\mu'} \to -g_{\mu\mu'} \qquad (19)$$

As indicated in [?], the right arrow indicates that this is not an actual equality, but the solution is valid as long as both sides are dotted into Eq. 17. The antisymmetric tensor, $\varepsilon_{\mu\nu\rho\sigma}\varepsilon^{\mu\nu}{}_{\rho'\sigma'}$ is simplified using Eq. A.30 of [?];

$$\varepsilon_{\mu\nu\rho\sigma}\varepsilon^{\mu\nu}{}_{\rho'\sigma'} = -2(g_{\rho\rho'}g_{\sigma\sigma'} - g_{\rho\sigma'}g_{\rho'\sigma}) \tag{20}$$

$$\tag{21}$$

Applying Eq. 20 to Eq. 18 results in;

$$|\mathcal{M}(P_P \to \gamma(p)\gamma(k))|^2 = |M_P|^2 (-2)(p^2 k^2 - (p \cdot k)^2) . \tag{22}$$

Substituting

$$(p + k)^2 = p^2 + k^2 + 2(p \cdot k) , \tag{23}$$

and applying $p^2 = k^2 = 0$, since both photons are massless because they are on-shell, we can derive the final expression of the squared amplitude of the decay $P_P \to \gamma(\epsilon_1, p)\gamma(\epsilon_2, k)$ as;

$$|\mathcal{M}(P_P \to \gamma(p)\gamma(k))|^2 = |M_P|^2 \frac{1}{2}(p + k)^4 = \frac{1}{2}|M_P|^2 m_P^4 \tag{24}$$

where m_P^4 is the mass of the η' derived from the 4-momenta conservation equation $(p + k)^4 = m_P^4$

A.1.2   Decay rate

The decay rate of a two-body decay is explained in Equation 46.17 of [?] as

$$d\Gamma = \frac{1}{32\pi^2} A |\mathcal{M}|^2 \frac{|\mathbf{p_1}|}{m_p^2} d\Omega , \tag{25}$$

where $d\Omega$ is the solid angle of particle 1 and A is the symmetry factor which appears because of the Bose symmetry of the two outgoing photons. Substituting the square matrix element from Eq. 24 into Eq. 25 and integrating over the solid angle yields;

$$\Gamma_{P\to\gamma\gamma} = \frac{1}{32\pi^2} \frac{1}{2} |\mathcal{M}(P_P \to \gamma(p)\gamma(k))|^2 \frac{|\mathbf{p}|}{m_P^2} 4\pi = \frac{1}{32\pi} |M_P|^2 m_P^2 |\mathbf{p}| \tag{26}$$

Finally, in the center-of-mass (C.M.) frame of the decaying meson, $\mathbf{p} = \mathbf{E}_\gamma^{\mathbf{C.M.}} = \frac{\mathbf{m_p}}{\mathbf{2}}$, we find the final expression of the decay rate of $P_P \to \gamma(\epsilon_1, p)\gamma(\epsilon_2, k)$ as;

$$\Gamma_{P\to\gamma\gamma} = \frac{1}{64\pi} |M_P|^2 m_P^3 . \tag{27}$$

A.2 $\phi \rightarrow \eta\gamma$ Decay

The $\phi \rightarrow \eta\gamma$ decay is analogous to the $\eta' \rightarrow \gamma\gamma$ decay by replacing the initial pseudoscalar meson P_p with a vector meson V_p and one of the γ propagators with η. In this substitution

$$\mathcal{M}(V_P(\epsilon_1) \rightarrow \eta(p)\gamma(\epsilon_2, k)) = M_V(p^2 = m_\eta, k^2 = 0)\varepsilon_{\mu\nu\rho\sigma}\epsilon_1^\mu p^\nu \epsilon_2^\rho k^\sigma \quad (28)$$

again, $\varepsilon_{\mu\nu\rho\sigma}$ is the antisymmetric metric tensor and the form factor, $M_V(p^2 = \eta, k^2 = 0)$, contains information of the $\phi - \eta$ transition.

A.2.1 *Decay rate*

The algebra for solving the squared matrix element is similar to Sec. A.1.1, however since now the initial meson has polarization, a factor of $1/3$ [?] is introduced. The decay rate is also similar within a factor of $1/3$ and can be represented as:

$$\Gamma_{V\rightarrow\eta\gamma} = \frac{1}{3}\frac{1}{64\pi}|M_V|^2 \left(\frac{m_\phi - m_\eta}{m_\phi}\right)^3 . \quad (29)$$

A.3 η' Dalitz Decay

When a pseudoscalar meson decays via a photon γ and a dilepton (l^+l^-) pair, it is known as a Dalitz decay or a so-called single off-shell decay. The Dalitz decay is related to the two photon decay. However, in the Dalitz decay, one of the photons is off-shell (γ^*) and decays into a dilepton pair. Since the Dalitz decay is related to the two photon decay, the form factor of the Dalitz decay, for $P(\eta')$, will be similar to the form factor of the two photon decay of $P(\eta')$, except there will be an effective mass dependence for the Dalitz decay. Figure 2b depicts the Feymann diagram of the Dalitz decay.

The amplitude for the decay $P_P \rightarrow \gamma^\star(p)\gamma(k) \rightarrow l^+(p_+)l^-(p_-)\gamma(k)$ is given by the following expression:

$$\mathcal{M}(P \rightarrow l^+(p_+, s_+)l^-(p_-, s_-)\gamma) = M_P(p^2, k^2 = 0)\varepsilon_{\mu\nu\rho\sigma}\frac{1}{q^2}e\bar{u}(p_-, s_-)\gamma^\mu v(p_+, s_-)q^\nu \epsilon^\rho k^\sigma.$$
$$(30)$$

Comparing the amplitudes of Eq. 30 and Eq. 15 it is seen that the polarization of the off-shell photon turned into the current $e\bar{u}(p_-, s_-)\gamma^\mu v(p_+, s_-)$ of the lepton pair. The parameters $s_\pm$ are the spin helicities of the outgoing leptons $l^\pm$ and as in Eq. 17, ϵ is the polarization of the outgoing photon.

A.3.1 *Squared Matrix Element*

$$\left|\mathcal{M}(P \to l^+(p_+, s_+)l^-(p_-, s_-)\gamma)\right|^2 =$$
$$\frac{e^2}{q^4}\left|M\right|^2 \varepsilon_{\mu\nu\rho\sigma}\varepsilon_{\mu'\nu'\rho'\sigma'}\bar{u}(p_-, s_-)\gamma^\mu v(p_+, s_+)\bar{v}(p_+, s_+)\gamma^{\mu'}u(p_-, s_-)q^\nu \epsilon^\rho k^\sigma q^{\nu'}\epsilon^{\rho'}k^{\sigma'}.$$

(31)

using an equation found between equation 5.3 and 5.4 found in [?]

$$\sum_{s_-, s_+}\bar{u}(p_-, s_-)\gamma^\mu v(p_+, s_+)\bar{v}(p_+, s_+)\gamma^{\mu'}u(p_-, s_-) = Tr\left[(\not{p}_- + m)\gamma^\mu(\not{p}_+ - m)\gamma^{\mu'}\right]$$
$$= 2q^2\left[-(g_{\mu\mu'} - \frac{p_\mu p_{\mu'}}{q^2}) - \frac{(p_+ - p_-)_\mu(p_+ - p_-)_{\mu'}}{q^2}\right]$$

(32)

where the identity $q = p_+ + p_-$ was used. Substituting Eq. 32 into Eq. 31

$$\left|\mathcal{M}\right|^2 = \frac{2e^2\left|M_P\right|^2}{q^2}\varepsilon_{\mu\nu\rho\sigma}\varepsilon_{\mu'\nu'\rho'\sigma'}\left[-g^{\mu\mu'} - \frac{(p_+ - p_-)^\mu(p_+ - p_-)^{\mu'}}{q^2}\right](-g^{\nu\nu'})q^\rho k^\sigma q^{\rho'}k^{\sigma'}$$

(33)

Substituting $k = P - q$ and $p_- = q - p_+$ into Eq. 33

$$\left|\mathcal{M}\right|^2 = \frac{2e^2\left|M_P\right|^2}{q^2}\varepsilon_{\mu\nu\rho\sigma}\varepsilon_{\mu'\nu'\rho'\sigma'}\left[-g^{\mu\mu'} - \frac{(2p_+ - q)^\mu(2p_+ - q)^{\mu'}}{q^2}\right]$$
$$\times (-g^{\nu\nu'})(q^\rho P^\sigma - q^\rho q^\sigma)(q^{\rho'}P^{\sigma'} - q^{\rho'}q^{\sigma'})$$

(34)

Applying properties of $-g^{\mu\mu'}$ and $-g^{\nu\nu'}$ onto Eq. 34

$$\left|\mathcal{M}\right|^2 = \frac{2e^2\left|M_P\right|^2}{q^2}\left[\varepsilon_{\mu\nu\rho\sigma}\varepsilon^{\mu\nu}{}_{\rho'\sigma'}q^\rho P^\sigma q^{\rho'}P^{\sigma'} + \frac{4}{q^2}\varepsilon_{\mu\nu\rho\sigma}\varepsilon^\mu{}_{\nu'\rho'\sigma'}p_+^\nu p_+^{\nu'}q^\rho q^{\rho'}P^\sigma P^{\sigma'}\right]$$

(35)

Switching to the rest frame of the pseudoscalar meson, P_p, the 4-momenta is transformed to $P^\sigma = m_p\delta^{\sigma 0}$. The squared amplitude of Eq. 35 reads;

$$\left|\mathcal{M}\right|^2 = \frac{2e^2\left|M_P\right|^2}{q^2}m_p^2\left[\varepsilon_{\mu\nu\rho}\varepsilon^{\mu\nu}{}_{\rho'}q^\rho q^{\rho'} - \frac{4}{q^2}\varepsilon_{\mu\nu\rho}\varepsilon^\mu{}_{\nu'\rho'}p_+^\nu p_+^{\nu'}q^\rho q^{\rho'}\right]$$

(36)

The sign change is due to $g^{\sigma\sigma'} = -\delta^{\sigma\sigma'}$. Using the antisymmetric tensor properties $\varepsilon_{\mu\nu\rho}\varepsilon^{\mu\nu}{}_{\rho'} = 2\delta_{\rho\rho'}$ and $\varepsilon_{\mu\nu\rho}\varepsilon^\mu{}_{\nu'\rho'} = \delta_{\nu\nu'}\delta_{\rho\rho'} - \delta_{\nu\rho'}\delta_{\rho\nu'} = (\hat{e}_\nu \times \hat{e}_\rho) \cdot (\hat{e}_{\nu'} \times \hat{e}_{\rho'})$, Eq. 36 is reduced to

$$\left|\mathcal{M}\right|^2 = \frac{2e^2\left|M_P\right|^2}{q^2}m_p^2\left[2\left|\mathbf{q}\right|^2 - \frac{4}{q^2}\left|\mathbf{q}\right|^2\left|\mathbf{p}_+\right|^2\sin^2(\theta_{p_+ q})\right]$$

(37)

A.3.2 Decay rate

The decay rate of a three-body decay is given in Equation 46.19 of [?] as

$$d\Gamma = \frac{1}{(2\pi)^5} \frac{1}{16m_p^2} |\mathcal{M}|^2 |\mathbf{p_1^*}| |\mathbf{p_3}| d\Omega_1^* d\Omega_3 dm_{12} , \qquad (38)$$

where $(|\mathbf{p_1^*}|, \Omega_1^*)$ is the momentum of particle 1 in the rest frame of 1 and 2, and Ω_3 is the angle of particle 3 in the rest frame of the decaying particle m_p [?]. Relating Eq. 38 to the variables in Eq. 37, where $(|\mathbf{p_1^*}|, \Omega_1^*) = (|\mathbf{p_+}|, \Omega_{p_+q})$, $m_{12} = q$ and $(|\mathbf{p_3}|, \Omega_3) = (|\mathbf{p_k}|, \Omega_k)$, reads;

$$d\Gamma = \frac{1}{(2\pi)^5} \frac{1}{16m_p^2} |\mathcal{M}|^2 |\mathbf{p_+}| |\mathbf{p_k}| d\Omega_+ d\Omega_k dq , \qquad (39)$$

In the rest from of the decaying particle m_p, the 3-momenta $|\mathbf{p_k}| = |\mathbf{q}|$ and the solid angle $\Omega_k = \Omega_q$. Substituting the square matrix element from Eq. 37 into Eq. 39 yields;

$$d\Gamma = \frac{1}{(2\pi)^5} \frac{1}{16m_p^2} \frac{2e^2 |M_P|^2}{q^2} m_p^2 \left[2|\mathbf{q}|^2 - \frac{4}{q^2} |\mathbf{q}|^2 |\mathbf{p_+}|^2 \sin^2(\theta_{p_+q}) \right] |\mathbf{p_+}| |\mathbf{q}| d\Omega_{p_+q} d\Omega_q dq . \qquad (40)$$

The variables $|\mathbf{q}|$ and $|\mathbf{p_+}|$ can be redefined, by means of Eq. 46.20b and Eq. 46.20a of [?], as

$$|\mathbf{q}| = \frac{m_p^2 - q^2}{2m_p} \qquad (41)$$

$$|\mathbf{p_+}| = \frac{\sqrt{q^2 - 4m_l^2}}{2} = \frac{q\sqrt{1 - \frac{4m_l^2}{q^2}}}{2} = \frac{q\mathcal{K}}{2} , \qquad (42)$$

where $\mathcal{K} = \sqrt{1 - \frac{4m_l^2}{q^2}}$. Replacing the variables calculated in Eq. 41 and Eq. 42 into Eq. 40 and collecting terms yields;

$$d\Gamma = \frac{1}{(2\pi)^5} \frac{1}{16m_p^2} |M_P|^2 \left[\frac{2e^2 m_p^2}{8} \left(\frac{m_p^2 - q^2}{2m_p} \right)^3 \right] \left(2 - \mathcal{K}^2 \sin^2(\theta_{p_+q}) \right) \frac{\mathcal{K}}{4q^2} dq^2 d\Omega_{p_+q} d\Omega_q , \qquad (43)$$

where the identity $qdq = \frac{dq^2}{2}$. Performing the integration of $\Omega_{p_+q} d\Omega_q$ and replacing $e^2 = 4\pi\alpha$ transforms Eq. 43 into;

$$d\Gamma = \frac{1}{(2\pi)^3} \frac{1}{32} \frac{4\pi\alpha}{3} |M_P|^2 \left[\frac{m_p^6 \left(1 - \frac{q^2}{m_p^2} \right)^3}{m_p^3} \right] (3 - \mathcal{K}^2) \frac{\mathcal{K}}{q^2} dq^2 , \qquad (44)$$

which can be simplified further to;

$$d\Gamma = \left(\frac{1}{64\pi}|M_P|^2 m_P^3\right) \frac{2\alpha}{3\pi} \frac{1}{q^2} \left(1 - \frac{q^2}{m_p^2}\right)^3 \left(1 + \frac{2m_l^2}{q^2}\right) \left(1 - \frac{4m_l^2}{q^2}\right)^{\frac{1}{2}} dq^2 .$$

(45)

It can be seen that the first set of variables in parenthesis in Eq. 45 is Eq. 27, therefore;

$$\frac{d\Gamma}{\Gamma_{\gamma\gamma}dq^2} = \frac{2\alpha}{3\pi} \frac{1}{q^2} \left(1 - \frac{q^2}{m_p^2}\right)^3 \left(1 + \frac{2m_l^2}{q^2}\right) \left(1 - \frac{4m_l^2}{q^2}\right)^{\frac{1}{2}}$$

(46)

which is the Kroll-Wada equation founded in [?].

A.4 ϕ Dalitz Decay

The amplitude for the decay $V_P \to \gamma^\star(p_1)\eta(p_2) \to l^+(p_+)l^-(p_-)\eta(p_2)$ is similar Eq. 30, but replacing the on-shell photon with an η:

$$\mathcal{M}(P \to l^+(p_+, s_+)l^-(p_-, s_-)\eta(p_2)) = M_P(p_1^2, p_2^2)\varepsilon_{\mu\nu\rho\sigma}\frac{1}{q^2}e\bar{u}(p_-, s_-)\gamma^\mu v(p_+, s_-)q^\nu\epsilon^\rho p_2^\sigma.$$

(47)

A.4.1 *Decay rate*

The decay rate for the ϕ transition to $\eta\gamma^\star$ is derived as [?]:

$$\frac{d\Gamma}{\Gamma_{\eta\gamma}dq^2} = \frac{\alpha}{3\pi} \frac{1}{q^2} \left(\left(1 + \frac{q^2}{m_\phi^2 - m_\eta^2}\right)^2 - \frac{4m_\phi^2 q^2}{m_\phi^2 - m_\eta^2}\right)^{\frac{3}{2}} \left(1 + \frac{2m_l^2}{q^2}\right) \left(1 - \frac{4m_l^2}{q^2}\right)^{\frac{1}{2}} ,$$

(48)

B Tabular Rates

Table 2 gives expected count rate for several bins of $M(e^+e^-)$ for a torus field setting of 75%. Table 3 gives expected count rate for several bins of $M(e^+e^-)$ for a torus field setting of 100%.

$M(e^+e^-)$ Bin Center	Upper	Uncertainty	Lower	Uncertainty
0.01	8924	94	946	31
0.03	1720	41	180	13
0.05	1041	32	113	11
0.07	758	28	84	9
0.09	578	24	62	8
0.11	479	22	54	7
0.13	411	20	45	7
0.15	369	19	37	6
0.17	329	18	36	6
0.19	317	18	36	6
0.21	280	17	30	5
0.23	268	16	28	5
0.25	250	16	26	5
0.27	269	16	28	5
0.29	266	16	24	5
0.31	250	16	25	5
0.33	240	15	24	5
0.35	258	16	25	5
0.37	309	18	31	6
0.39	280	17	28	5
0.41	352	19	35	6
0.43	285	17	31	6
0.45	299	17	31	6
0.47	315	18	34	6
0.49	328	18	35	6
0.51	326	18	38	6
0.53	331	18	30	5
0.55	282	17	28	5
0.57	401	20	38	6
0.59	416	20	45	7
0.61	438	21	48	7
0.63	445	21	44	7
0.65	448	21	44	7
0.67	577	24	63	8
0.69	689	26	69	8
0.71	728	27	79	9
0.73	716	27	71	8
0.75	706	27	73	9
0.77	565	24	54	7
0.79	277	17	29	5
Total	26521	163	2784	53

Table 2: Counts rates for bins of $M(e^+e^-)$ at 75% torus field

$M(e^+e^-)$ Bin Center	Upper	Uncertainty	Lower	Uncertainty
0.01	7937	89	859	29
0.03	1516	39	163	13
0.05	934	31	102	10
0.07	684	26	77	9
0.09	501	22	56	7
0.11	392	20	45	7
0.13	366	19	40	6
0.15	335	18	34	6
0.17	276	17	31	6
0.19	266	16	30	5
0.21	246	16	28	5
0.23	238	15	25	5
0.25	218	15	22	5
0.27	245	16	26	5
0.29	225	15	21	5
0.31	218	15	22	5
0.33	217	15	22	5
0.35	226	15	23	5
0.37	275	17	29	5
0.39	256	16	27	5
0.41	292	17	31	6
0.43	274	17	29	5
0.45	262	16	26	5
0.47	244	16	27	5
0.49	296	17	32	6
0.51	303	17	36	6
0.53	295	17	28	5
0.55	255	16	26	5
0.57	338	18	33	6
0.59	381	20	43	7
0.61	382	20	43	7
0.63	399	20	41	6
0.65	419	20	41	6
0.67	527	23	57	8
0.69	597	24	62	8
0.71	695	26	76	9
0.73	664	26	68	8
0.75	657	26	68	8
0.77	545	23	54	7
0.79	271	16	28	5
Total	23667	154	2528	50

Table 3: Counts rates for bins of $M(e^+e^-)$ at 100% torus field